BULLETIN OF THE POLISH ACADEMY OF SCIENCES
TECHNICAL SCIENCES, Vol. 73(5), 2025, Article number: e154722
DOI: 10.24425/bpasts.2025.154722

Direct speed finite control set model predictive control for PMSM drive – robustness analysis

Hubert LISIŃSKI* and **Tomasz TARCZEWSKI**

Institute of Engineering and Technology, Nicolaus Copernicus University in Torun, ul. Grudziadzka 5, 87-100 Torun, Poland

Abstract. Currently, high-performance electrical drives with advanced control schemes are presented in the literature. Many of them will not be used in the industry because of implementation issues or difficulties in the optimal selection of control parameters. In this paper, two different model predictive control (MPC) schemes are developed for PMSM drive and compared in experimental tests both in time and frequency domains. To provide high-performance operation of the drive, a complex cost function is constructed, and a metaheuristic optimization algorithm is utilized for the automatic selection of weighting factors. Developed control schemes were implemented in a microprocessor-based prototype drive and examined in terms of robustness for three different moments of inertia. Trajectory tracking ability for step and ramp reference angular velocity, as well as load torque compensation, have also been investigated. The study makes an important contribution as a reliable and robust model predictive control scheme for PMSM drive with potential for industrial applications.

Keywords: model predictive control; PMSM drive; metaheuristic optimization algorithm; robustness.

1. INTRODUCTION

Modern electrical drives must meet several expectations, such as superior trajectory tracking, disturbance compensation, robustness against parameter uncertainties, and energy efficiency. To meet the above-mentioned requirements, high-performance permanent magnet synchronous motors (PMSMs) and novel, advanced control schemes are proposed [1]. One of the most promising and developing approaches is model predictive control (MPC) [2]. It is caused by several advantages of MPC, such as intuitive concept, the inclusion of constraints and nonlinearities, and relatively simple implementation of the resulting controller [3]. On the other hand, the control performance depends on the model quality, and computational complexity is higher compared to a classic control scheme [4]. The robustness against parameter changes is also a challenge [2]. MPC has recently been applied to electromobility, unmanned aerial vehicles, ship control, and blade pitch control of wind turbines [5–7]. In [5], MPC is used to adjust torque for wheel speed relies on steering wheel position, accelerator pedal, and car dynamics parameter. In this approach, energy losses and tire longitudinal slip are applied in the cost function. Unfortunately, the computational complexity of this approach is large. In [6], an inner control loop responsible for attitude control is based on the MPC approach. In the outer position control loop, an optimal backstepping controller was implemented. The latter control loop requires coefficients to be tuned. Therefore, genetic algorithm has been used as a metaheuristic tool to solve this problem. As shown in [6], hybrid control structures with MPC in the inner loop enhance control performance compared to classic approaches, but selecting a complex outer controller requires expert knowledge. In [7], MPC used to adjust the blade pitch of a wind turbine, while a PI-based torque controller operates in parallel. The MPC structure also includes a preview filter and a state constructor, which operates in a feedback loop with MPC. The authors reported satisfactory performance, but the computational burden is high, and no sensitivity analysis was conducted

MPC is still being developed, and two main directions can be identified. In the finite control set (FCS) approach, where the number of possible solutions is limited, further optimization of the search procedure is desired. In the classical FCS method applied for the power converter or electrical drive control, full voltage vectors are taken [2–4]. This means that power transistors are opened for the whole sampling time, and a space vector modulator (SVM) does not need to be used. The number of vectors depends on the inverter topology. For a most popular 2-level voltage source inverter (VSI), 8 vectors are available, but the computational complexity increases with the increase of the prediction horizon. To overcome this disadvantage, an optimization of the search procedure is proposed. For example, in [8], the selection of the voltage sector is based on deadbeat control theory. This approach simplifies FCS but introduces some limitations, such as higher dependency on the model, which increases sensitivity to parameters mismatch, for example, inductances or inertia. This problem may cause lower performance. In the continuous control set (CCS) MPC, a better solution can be found since the whole space is searched. Several optimization algorithms are used in this approach, for example, quadratic programming (QP) [9]. In this method, it is possible to introduce constraints in a simple way. On the other hand, the computational burden of the proposed is 24.8 μs, and

*e-mail: hubert.lisinski@umk.pl

Manuscript submitted 2025-03-28, revised 2025-03-28, initially accepted for publication 2025-05-11, published in August 2025.

there is no information about the outer controller used. In [10], it was shown that FCS MPC could give a similar performance and lower complexity than CCS MPC with the QP algorithm. In this solution, a cascade structure with both angular velocity and torque MPC controllers is proposed for the induction motor. It was found that the FCS provides a better torque capability at high-speed levels compared to CCS. Moreover, the outer loop performance is related to the inner loop method. Other optimization approaches were presented in [11]. In this approach, several methods and MPC structures are compared in terms of computational complexity. Sequential MPC is used, and it should be treated as a cascade approach that affects the system dynamics. In this concept, establishing priority control for the investigated model is essential. A relevant example is a wind turbine application presented in [12]. In that study, MPC was applied to both the motor and the inverter, with the cost function in one case based on voltage and in the other on switching frequency. Despite the structural diversity of MPC, the most common approach is referred to as simplified model-based MPC in [11]. In the literature, MPC structures typically involve current prediction, while speed prediction is often omitted, with control handled by a PI regulator [13, 14]. However, these studies provide no justification for the use of PI control. The focus is primarily on current performance, likely leading to the exclusion of speed considerations—an issue in real applications, such as in [14], where the motor operates as a wind turbine. An alternative is full MPC, which, unlike the simplified version, includes speed prediction [15]. Here, the authors propose a speed prediction method based on a third-order Taylor series expansion and present robustness test results where friction was varied. However, they do not explain why direct speed MPC was chosen over model predictive current control with a PI speed regulator.

A key element of MPC is the cost function, which defines the influence of various factors on regulation. Different cost function designs exist in the literature. A common approach uses dq-axis current, comparing measured and predicted values [16]. Its advantage is simple measurement and prediction, but it lacks direct torque and flux control. To address this, some researchers use torque and flux instead [17], though this increases computational complexity and estimation challenges. One benefit of cost functions is their flexibility in incorporating additional components. For example, the mean square error (MSE) criterion [18] improves tracking accuracy and is referred to as a target-oriented method. Finite control set MPC eliminates the need for a modulator, reducing computational complexity. However, maintaining a constant switching frequency requires alternative methods. Researchers often add a term to the cost function to account for transistor switching [19]. In [19], three cost function designs were compared, showing that precise formulations lower switching frequency while maintaining accuracy. Cost functions for current control are more complex than those for speed control, where the cost function simply compares the reference and predicted values. The main difference in speed control methods lies in speed prediction, while in current-based cost functions, only the reference value for q-axis current is adjusted.

Many studies on MPC focus on robustness to inductance variations, while the impact of inertia changes and reference speed frequency variations is often overlooked [20]. This omission is primarily due to technical challenges, such as the difficulty of modifying test benches for such studies. While real-world applications like robots or CNC machines could provide better insights, they are costly. Additionally, traditional controllers are often combined with adaptive methods like recursive least squares (RLS) or the Kalman filter, reducing the need for direct inertia robustness analysis. Some researchers address robustness issues using RLS adaptation with classical input-output-error data, fuzzy logic, or multi-layer neural networks [21, 22]. In [21], a fuzzy logic–neural network hybrid optimizes the cost function, improving rise time. In [22], adaptive RLS-based systems were compared with classical PI regulators across various models, showing enhanced robustness. Robustness is typically evaluated via time response; however, this study proposes Bode characteristic analysis. Frequency response was examined under two conditions: a sinusoidal reference signal and a sinusoidal load torque at zero speed. While this method provides high robustness, it significantly increases computational complexity. In applications with rapid and substantial variations, selecting a more resilient controller becomes essential.

In advanced control systems, the cost function is often significantly extended, for example, in multi-level inverters and advanced battery management systems [23, 24]. In such cases, applying weighting factors is necessary. However, tuning them can be challenging, making this an ideal area for nature-inspired optimization algorithms. MPC commonly employs particle swarm optimization (PSO) [25], and genetic algorithms (GA) [26] to address this issue. The latter demonstrates how weighting factors of additional cost function components—such as switching frequency and DC grid ripple—can be optimized using a genetic algorithm. To minimize ripple, the authors measured the total harmonic distortion (THD) indicator and included it in the GA cost function. In [25], PSO is used to tune flux and switching frequency weighting factors. The sequential MPC method discussed earlier, does not require weighting factors, as priorities are determined by the sequential structure. Meanwhile, other control methods, such as SFC, CCS, or multiresonant controllers, utilize different optimization techniques, including the artificial bee colony (ABC) algorithm [27], a grey wolf optimizer (GWO), and a PSO [28].

Recent advancements in model predictive control (MPC) for electric drives have emphasized the integration of high-performance hardware platforms to meet real-time computational demands. Studies have demonstrated the efficacy of field-programmable gate arrays (FPGAs) and high-speed digital signal processors (DSPs) in executing complex MPC algorithms with reduced latency, catering to applications requiring high control frequencies [29]. For instance, the utilization of OPAL-RT systems has been validated for implementing robust MPC strategies in permanent magnet synchronous motors (PMSMs), ensuring accurate real-time emulation and effective handling of load variations [30]. Additionally, simulation environments like MATLAB/Simulink and PLECS have been employed for

the development and testing of MPC schemes, facilitating the transition from theoretical models to practical applications [31]. These platforms collectively contribute to the advancement of MPC in electric drive systems by providing reliable and efficient means for real-time control implementation.

Summary literature overview, the majority of papers about MPC structure focused on the current control loop. If authors decide to make a robustness analysis, they usually investigate inductance or resistance variations. Research usually are based on time responses, fast Fourier transformation, and the THD indicator. The frequency response is skipped, while the comparison includes different MPC approaches. Therefore, in this paper, the authors decided to investigate PI-MPCC and DS-MPC in terms of the moment of inertia and reference speed frequency variations. To the best of the author's knowledge, ABC was not used for MPC weighting factors tuning, so in this paper, it is presented. That decision was made because ABC has shown promising results in other optimization contexts. ABC mimics the foraging behavior of honeybees to search for optimal solutions in high-dimensional spaces, making it well-suited for the complex optimization required in MPC tuning. MPC structure with optimally selected weighting factors was chosen.

This paper is divided into six sections. In Section 2, a mathematical model of PMSM is described. Section 3 presents the proposed DS-MPC control method, while Section 4 focuses on the ABC tuning algorithm. Experimental results for the investigated method and reference PI-MPCC-based solution are shown in Section 5. Here, robustness analysis in the time and frequency domain is included. The conclusion is presented in Section 6.

2. MODEL OF PMSM

Since MPC requires a model of the plant to calculate future states for optimization tasks, electrical and mechanical differential formulas describing considered machines need to be introduced. These are as follows

$$\frac{d\psi_d(t)}{dt} = u_d(t) - Ri_d(t) + p\omega(t)\psi_q(t), \tag{1}$$

$$\frac{d\psi_q(t)}{dt} = u_q(t) - Ri_q(t) - p\omega(t)\psi_d(t), \tag{2}$$

$$J\frac{d\omega(t)}{dt} = T_e(t) - B\omega(t) - \hat{T}_L(t) - F_c\text{sign}\big(\omega(t)\big), \tag{3}$$

where $u_d(t)$, $u_q(t)$, $i_d(t)$, $i_q(t)$ – voltage, current components in the direct and quadrature axis, R – stator resistance, ψ_f – magnet flux, p – number of pole pairs, $\omega(t)$ – rotational velocity of the rotor, J – moment of inertia, B – viscous friction coefficient, $\hat{T}_L(t)$ – estimated load torque, F_c - static friction coefficient. In order to develop current control, it is necessary to substitute flux with respective currents

$$\psi_d(t) = L_d i_d(t) + \psi_f\,, \tag{4}$$

$$\psi_q(t) = L_q iq(t). \tag{5}$$

Finally, the formula describing the electromagnetic torque should be introduced

$$T_e = \frac{3}{2}p\Big[\psi_f i_q(t) + \Big(L_q - L_d\Big)i_d(t)i_q(t)\Big]. \tag{6}$$

Since the proposed control scheme will be developed for PMSM with surface-mounted permanent magnets, the following simplification can be made: $L_s = L_q = L_d$. Finally, the model of the PMSM described in the continuous time domain is as follows:

$$\frac{di_d(t)}{dt} = \frac{K_p}{L_s}u_d(t) - \frac{R}{L_s}i_d(t) + p\omega(t)i_q(t), \tag{7}$$

$$\frac{di_q(t)}{dt} = \frac{K_p}{L_s}u_q(t) - \frac{R}{L_s}i_q(t) - \frac{p\psi_f}{L_s}\omega(t) - p\omega(t)i_d(t), \tag{8}$$

$$J\frac{d\omega(t)}{dt} = \frac{3}{2}p\psi_f i_q(t) - B\omega(t) - \hat{T}_L(t) - F_c sign\Big(\omega(t)\Big). \tag{9}$$

From (7)–(8), it can be seen that non-linearity and cross-coupling exist. Such phenomena are problematic for FOC with linear PID-based controllers, and these require a decoupling method, as shown in [1]. In the case of MPC structure, the above-mentioned drawback is not a key since this control scheme can be directly developed for a non-linear model.

Finally, a discrete form of the PMSM model should be determined. After the application of the Tustin method, the following model is obtained:

$$i_d(k+1) = x_1 u_d(k) + x_2 i_d(k) + x_3\omega(k)i_q(k), \tag{10}$$

$$i_q(k+1) = x_1 u_q(k) + x_2 i_q(k) - x_3\omega(k)i_d(k) - x_4\omega(k) \tag{11}$$

with

$$x_1 = \frac{T_s}{L_s}, \quad x_2 = \left(1 - R\frac{T_s}{L_s}\right), \quad x_3 = pT_s, \quad x_4 = p\psi_f\frac{T_s}{L_s},$$

where T_s – the discrete sample time.

$$\omega(k+1) = \left(1 - \frac{T_s B}{J}\right)\omega(k) + \frac{T_s}{J}\Big(K_t i_q(k) - \hat{T}_l(k) - F_c\text{sign}\Big(\omega(k)\Big)\Big). \tag{12}$$

3. MODEL PREDICTIVE CONTROL OF PMSM

As described before, MPC is a flexible control structure that allows for the use of different approaches to voltage vector selection. In the literature, the most popular methods are FCS, CCS, or deadbeat control (DBC) [8]. Due to the low complexity, it was decided to use FCS in this paper. In its basic form, FCS utilizes all possible states of the VSI power transistors. In this approach, a space vector modulator (SVM) is not necessary, and selected transistors are opened for the entire time period (i.e., the sampling time). The lack of SVM was somewhat important in the past due to the low computational abilities of the microprocessors. Currently, SVM is applied to mitigate current ripples, noise, and vibrations of the motor.

3.1. Current prediction

In the MPC scheme, the prediction of future plant states plays an essential role. The simplest way to obtain predicted state variables is to discretize the model containing differential ordinary equations. For the considered PMSM drive, discrete equations were presented in (10) and (11). However, it is worth noting that the MPC scheme computational complexity is high, so measurement delays may appear. In order to overcome this flaw, the current is usually predicted for two-time samples ahead. During this prediction, it is assumed that the speed and voltage set remain constant, resulting in following formulas

$$i_d(k+2) = x_1 u_d(k+1) + x_2 i_d(k+1) + x_3 \omega(k) i_q(k+1), \tag{13}$$

$$i_q(k+2) = x_1 u_q(k+1) + x_2 i_q(k+1) - x_3 \omega(k) i_d(k+1) - x_4 \omega(k). \tag{14}$$

3.2. Speed prediction

As stated before, the direct speed FCS-MPC is proposed in this approach. Due to this, it is necessary to obtain the future value of the angular speed. Similar to the current prediction described before, the simplest way to predict the speed is to discretize (12). Here, it was decided to adapt the 3rd Taylor series discretization proposed in [15]:

$$\omega(k+2) = y_1 i_d(k+1)\omega(k) + y_2 i_q(k+1) + y_3 \omega(k) + y_4 \hat{T}_L(k) + y_5 u_q(k+1) \tag{15}$$

with

$$y_1 = \frac{-3\psi_f T_s^2 p^2}{4J}, \quad y_2 = \frac{3\psi_f T_s p}{2J} - 3T_s^2 \psi_f p \frac{\frac{3B}{2J^2} + \frac{R}{2JL_s}}{2},$$

$$y_3 = 1 - \frac{3T_s B}{J} + T_s^2 \frac{\frac{B^2}{J^2} - \frac{3p^2\psi_f^2}{2JL_s}}{2},$$

$$y_4 = \frac{T_s^2 B}{2J^2} - \frac{T_s}{J}, \quad y_5 = \frac{3\psi_f T_s^2 p}{4JL_s}.$$

3.3. Direct speed control structure

In direct speed MPC, it is necessary to calculate the reference values of currents. Since a surface-mounted permanent magnet machine is considered here, it is reasonable to implement a control strategy with zero d-axis current. In the case of q-axis current, the formula based on (12) was used [15]

$$i_{q\text{ref}} = \frac{B\omega_{\text{ref}}(k)}{K_t} + \frac{\hat{T}_L(k)}{K_t} + \frac{F_c}{K_t}\text{sign}(\omega(k)) + K_{ff} \tag{16}$$

with

$$K_{ff} = K_g \frac{\omega_{\text{ref}}(k) - \omega_{\text{ref}}(k-1)}{T_s}.$$

One can see that the above-mentioned formula refers to $i_{q\text{ref}}$ in steady-state because it has to compensate for all kinds of disturbances (e.g., friction) in the system. Since steady-state is considered, the left side of (9) is omitted, and the moment of inertia does not affect $i_{q\text{ref}}$. Finally, to improve dynamics properties for a higher order reference signal (e.g., ramp) and to compensate back-emf, a feedforward path with gain coefficient K_g and ω_{ref} was introduced.

In the next step, a cost function must be constructed. Since it will be optimized to provide a high-performance drive operation, it should contain components related to the most important requirements, such as [32] (i) steady-state error-free angular velocity and q-axis current control, (ii) zero d-axis current control strategy, (iii) low level of the current and the velocity ripples and, (iv) current limitation in transient. Therefore, the following formula was proposed

$$f_{\text{cost}} = W_w c_\omega + W_d c_{i_d} + W_q c_{i_q} + W_{\text{limit}}, \tag{17}$$

where

$$c_\omega = \left(\omega_{\text{ref}} - \omega(k+2)\right)^2, \tag{18}$$

$$c_{i_d} = \left(i_d(k+2)\right)^2, \tag{19}$$

$$c_{i_q} = \left(i_{q\text{ref}} - i_q(k+2)\right)^2, \tag{20}$$

$$W_{\text{limit}} = \begin{cases} \infty & \text{for } |i_s(k+1)| \geq i_N, \\ 0 & \text{for } |i_s(k+1)| < i_N, \end{cases} \tag{21}$$

where W_w, W_d, W_q – weighting coefficients, i_s – stator current, i_N – rated stator current. One can see that several weighting coefficients are introduced in (17). Their values will be automatically selected using a metaheuristic optimization algorithm. The procedure will be described in the following section. The scheme of the described control algorithm is presented in Fig. 2a.

4. TUNING OF WEIGHTING FACTORS

From (21), it can be seen that values of weighting coefficients need to be chosen to provide high-performance drive behavior. As mentioned before, the considered task can be accomplished using a metaheuristic optimization algorithm. As shown in [33], such algorithms are used due to better convergence and robustness against local minima compared to the exact optimization methods. Recently, several metaheuristic optimization algorithms (e.g., PSO, GA) have been used in electrical drive applications [25, 26]. In this paper, it was decided to apply ABC optimization algorithm. It was selected because of the confirmed convergence and repeatability of results obtained in similar tasks [27]. The general principle of ABC operation is presented in Fig. 1. It is worth noting that in all phases of the optimization, the cost function is minimized. Here, it was decided to develop the cost function based on the *ISE* performance index, and this is as follows:

$$f_{ABC} = \alpha ISE_\omega + \beta ISE_q + \gamma ISE_d \tag{22}$$

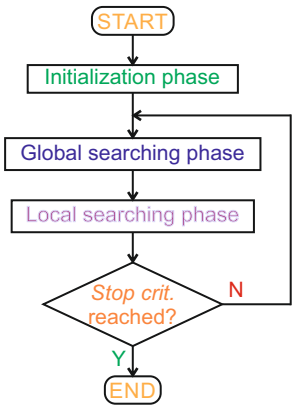

Fig. 1. General flowchart of ABC optimization algorithm

with

$$ISE_\omega = \sum_{g=0}^{N} \Big(\omega_{\text{ref}}(g) - \omega(g)\Big)^2 T_s,$$

$$ISE_d = \sum_{g=0}^{N} i_d(g)^2 T_s\,,$$

$$ISE_q = \sum_{g=1}^{N} \frac{\Big(i_q(g) - i_q(g-1)\Big)^2}{T_s}\,,$$

where $\alpha = 1$, $\beta = 0.01$, $\gamma = 0.05$ – manually selected weighting factors. After analysis of (17) and (22), one can see that the same number of coefficients (three in this particular case) must b chosen. On the other hand, the manual selection of ABC weighting factors seems to be simpler since each of them independently influences the measured currents and speed in the optimization process. The procedure is more intuitive since the user only needs to define values that determine the individual approximate impact of currents and speed on the optimization outcome. Such an approach is more universal since it can be applied to tuning more complex cost functions and hybrid regulators, which will be presented in the later part of this paper. The tuning process was carried out using a MATLAB environment, but data was collected from the experimental setup described in this paper. The control parameters of ABC are listed in Table 1. As a stop criterion indicated in Fig. 1, the maximum number of iterations equal to 10 was set.

Table 1
The control parameters of ABC

Parameter	Value
Colony size	30
Food number	15
Modification rate	0.8
Scout production period	45
Control parameter	45
Lower bound of all parameters	$1.0 \cdot 10^{-3}$
Upper bounds of W_d and W_q	$15.0 \cdot 10^{3}$
Upper bounds of W_w	$40.0 \cdot 10^{5}$

5. EXPERIMENTAL RESULTS

5.1. Laboratory setup

The developed control scheme was investigated in the laboratory stand with two PMSM drives. The main drive is fed by a two-level VSI with SiC power devices. The control algorithm is implemented in an ARM microcontroller with a Cortex 4 core from STMicroelectronics. The second drive is controlled by commercial VSI, and it is used to generate load torque. Both motors are connected using a clutch and a mechatronic system that allows for changes in the moment of inertia. The laboratory setup is presented in Fig. 3, and the parameters of the main PMSM drive are defined in Table 2. Current and voltage measurements were performed using LEM LTS15NP and LV25P transducers, respectively. Position measurement was ensured by

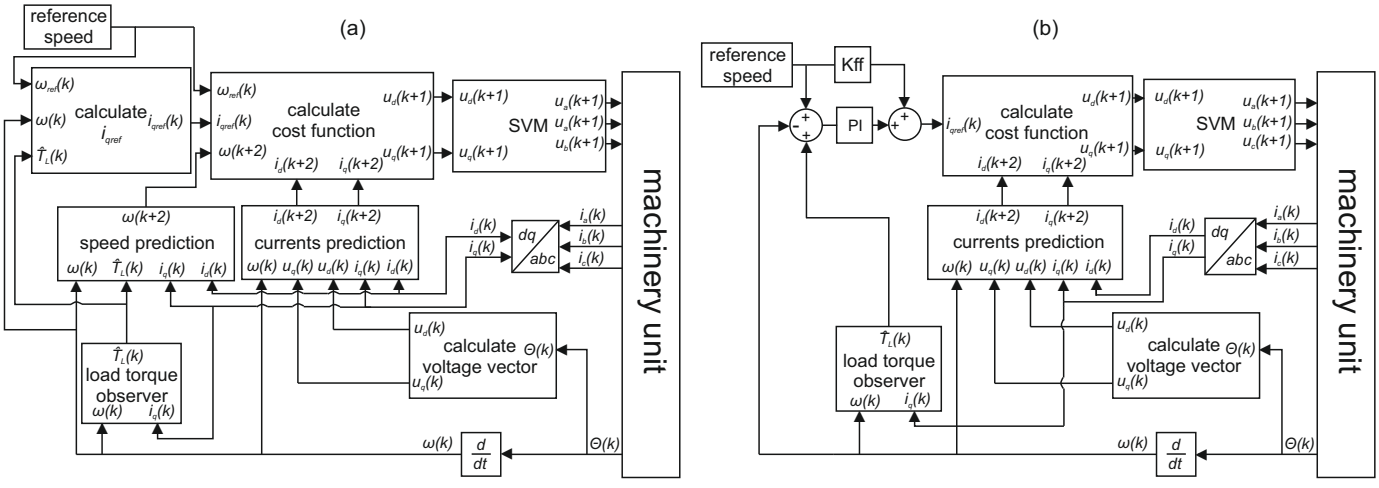

Fig. 2. Block diagrams of considered control structures with MPC – model predictive control, PI – speed controller, SVM – space vector modulator: (a) DS-FCS-MPC, (b) PI-FCS-MPCC

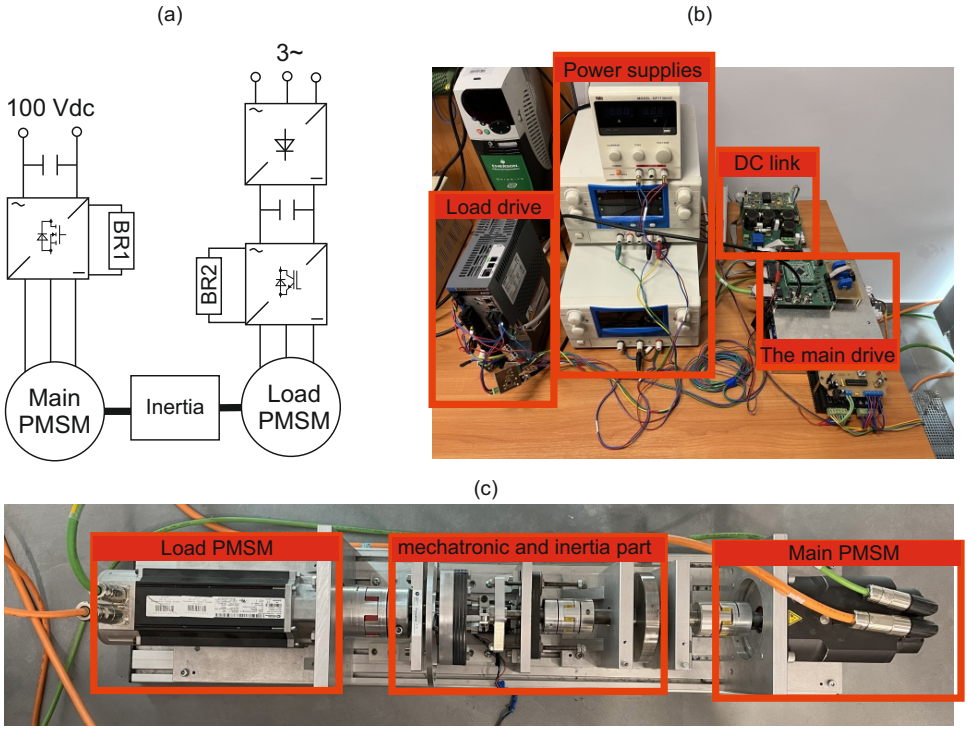

Fig. 3. The experimental setup with: (a) simplified electrical scheme, (b) power supplies and drive, (c) machinery unit

Table 2
Selected parameters of PMSM drive

Parameter	Symbol	Value & Unit
Rated angular velocity	ω_N	300 rad/s
Rated current	i_N	5 A
Minimal moment of inertia	$J_{\min}$	$7.2 \cdot 10^{-3}$ kgm^2
Nominal moment of inertia	J_{nom}	$17.7 \cdot 10^{-3}$ kgm^2
Maximal moment of inertia	$J_{\max}$	$31.3 \cdot 10^{-3}$ kgm^2
Viscous friction	B	$1.4 \cdot 10^{-2}$ Nms/rad
Static friction	F_c	$30.4 \cdot 10^{-2}$ Nms/rad
Torque constant	K_t	1.14 Nm/A
Switching frequency	f_s	10 kHz

a Stick Stegmann SRS50 absolute encoder. The load PMSM drive was controlled via a Kollmorgen AKD drive.

The implementation of MPC algorithm is presented in Algorithm 1. At the beginning of each iteration, auxiliary variables—such as the minimum value for the optimization loop and the initial cost function value—are initialized. Next, reference speed values are determined based on the selected slope, using an appropriate structure. In the following step, the candidate voltage vectors are generated. This procedure relies on calculating the dq-axis voltages from constant $\alpha\beta$-axis voltages and the rotor angle, using the Clarke–Park transformation. The resulting set of voltage candidates is then processed in an optimization loop, where the values of u_d and u_q yielding the lowest cost function value are stored. Upon completion of the loop, the optimal voltages are passed to the space vector modulation (SVM) module, which computes the transistor switching

Algorithm 1. MPC implementation algorithm

$f_{\text{cost}}^{\min} = \infty$
$u_q^{\text{opt}} = 0$
$u_d^{\text{opt}} = 0$
$T_{cnt} = T_{cnt} + T_s$
$\omega_{\max} = 10$ ▷ maximal reference speed
if αT_{cnt} is greater than $\omega_{\max}$ **then**
  $\omega_{\text{ref}} = \omega_{\max}$
else
  $\omega_{\text{ref}} = \alpha T_{cnt}$
end if
Calculation of $i_d(k+1)$ and $i_q(k+1)$ for delay compensation, as well as other variables such as load torque and reference current.
$m = 0$
for m smaller than 7 **do**
  calculation $id(k+2)$, $iq(k+2)$ and $\omega(k+2)$
  from (13)–(15), as well as f_{cost} from (17) or (23)
  if f_{cost} is smaller than $f_{\text{cost}}^{\min}$ **then**
    $f_{\text{cost}}^{\min} = f_{\text{cost}}$
    $u_q^{\text{opt}} = u_q(m)$
    $u_d^{\text{opt}} = u_d(m)$
  end if
  $m = m + 1$
end for
send u_q^{opt} and u_d^{opt} to invert Clarke-Park transformation and SVM.

times. Additionally, it is worth noting that measurements are triggered by an interrupt on the microcontroller at the midpoint of the PWM cycle. This ensures acquisition of averaged current values and mitigates ripple effects caused by the structure of the VSI and the switching frequency. Immediately after the measurements are completed, the control algorithm is executed.

As described before, the ABC optimization algorithm has been used to optimal tune coefficients of the cost function (17), and obtained values are listed in Table 3. For the sake of comparison, the proposed control scheme was confronted with a reference solution, namely a cascade structure with FCS-MPCC inner current control loop and PI-based angular velocity controller. This is shown in Fig. 2b. As in the case of the developed direct speed MPC, a similar cost function has been used

$$f_{\text{cost}} = W_d c_{i_d} + W_q c_{i_q} + W_{\text{limit}}\,. \tag{23}$$

Also here, coefficients were selected using the ABC-based optimization method. Its values, along with automatically selected PI controller coefficients, are listed in the last column in Table 3.

Table 3
Value of weighting factors for DS-FCS-MPC and PI-FCS-MPCC structure

Symbol of coefficient	DS-FCS-MPC	PI-FCS-MPCC
K_P	–	1.4866
K_I	–	87.7740
W_ω	1516200	–
W_q	3149.8	121380
W_d	13136.9	65552

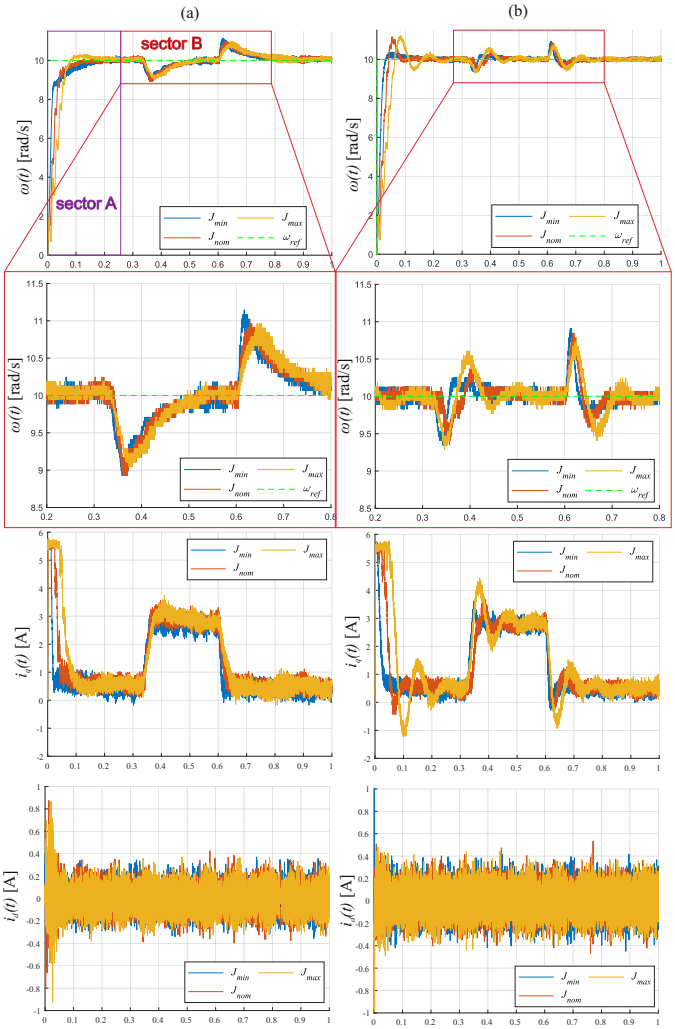

Fig. 4. Time responses for speed reference value set to 10 rad/s and different moments of inertia: (a) DS-FCS-MPC, (b) PI-FCS-MPCC

5.2. Time responses

This subsection presents drive responses for step and ramp reference signals. In the first case, experiments were conducted for $\omega_{\text{ref}} = 10$ rad/s, and $T_l = 2$ Nm. The load torque was imposed at $t = 0.35$ s and removed at $t = 0.6$ s. Firstly, it is important to consider Fig. 4, which shows how DS-FCS-MPC and PI-FCS-MPCC work for different moments of inertia. From Fig. 4b, it can be seen that the overshoot exists for all moments of inertia. Such behavior results in a better load torque compensation, but it is also responsible for oscillations observed in ω_m and i_q, resulting in longer transient. In the second row in Fig. 4, enlarged parts of angular speed for PMSM with imposed load torque are presented. From the obtained results, it can be seen that the DS-FCS-MPC control structure gives more predictable responses for different moments of inertia. The above-described observation is confirmed by the parameters listed in Table 4. The rise time t_r is lower for PI-FCS-MPCC than for DS-FCS-MPC, independently of the moment of inertia. On the other hand, t_r values change less between different moments of inertia for DS-FCS-MPC. The steady-state time t_{st} is shorter for PI-FCS-MPCC than for DS-FCS-MPC in the case of J_{nom}, but for a changed moment of inertia, the t_{st} of PI-FCS-MPCC is longer than that of the opposite method. DS-FCS-MPC exhibits lower t_{st} variation for different moments of inertia, similar to t_r. The overshoot for load torque M_{load} is definitely lower for the scheme with a PI controller than for direct speed control. Summarizing the above analysis, PI-FCS-MPCC has a higher potential for faster and more rapid load torque compensation, while DS-FCS-MPC has greater robustness to moment of inertia variations.

Figure 5 presents a response test system for a ramp input signal. In order to achieve perfect tracking of the reference sig-

Table 4
Selected parameters of time responses

parameter	DS-FCS-MPC			PI-FCS-MPCC		
	J_{min}	J_{nom}	J_{max}	J_{min}	J_{nom}	J_{max}
t_r [s]	42.2	42.4	59.4	22.2	34.8	53.8
t_{st} [s]	142.7	97.5	152.6	146.5	81.6	197.5
M_{load} [rad/s]	1.012	0.845	0.832	0.845	0.619	0.624

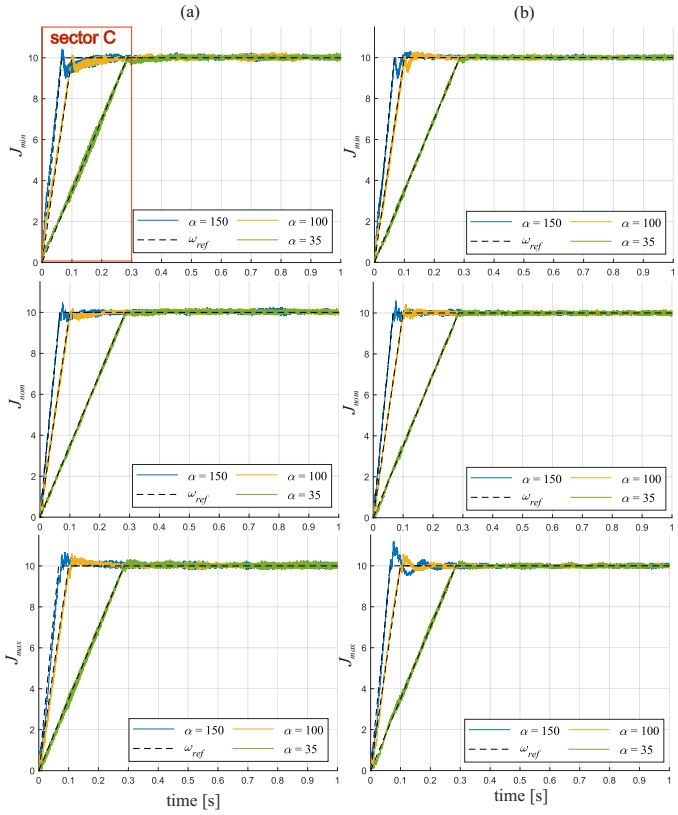

Fig. 5. PMSM drive responses for ramp acceleration with different slope angles and three moments of inertia: (a) DS-FCS-MPC, (b) PI-FCS-MPCC

nal in transient, it was necessary to add feedforward gain in i_{qref} signal (16)) and in PI structure. The value of K_g was determined experimentally to obtain the best possible performance of the drive and finally set to 0.02.

To begin with, one should look at signals for J_{nom}. It is possible to notice a great tracking trajectory for both controllers. Differences appear for mismatch moment of inertia. It can be observed that DS-FCS-MPC is less sensitive to changes in motor parameters. This is particularly evident for J_{max}. At this point, it is worth noting that both controllers did not provide ideal trajectory tracking without feedforward. Looking at Fig. 5 it can be noticed that problems appear for the ramp with a small slope. Therefore, it was decided to carry out frequency research. To provide a precise analysis, robustness indicators were calculated for transient with α equal to 150, and respective results are presented in the following subsection.

5.3. Robustness analysis

To further investigate the robustness of the developed predictive control schemes, the performance indicators have been introduced. These are based on the mean square error (MSE). In the first step, MSE for the angular velocity speed was calculated for the considered set of the moment of inertia.

$$MSE_j = \frac{1}{N}\sum_{g=kT_s}^{N}\left(p_g^j - p_g^{j_{\text{ref}}}\right)^2, \tag{24}$$

where N – number of samples, p_g^j – value of measured parameters, $j = i_s, \omega$ in g-th sample time, $p_g^{j_{\text{ref}}}$ – value of respective reference signal, $k = 1, 2, \ldots N$. In the next step, percentage errors in relation to nominal value were calculated.

$$\delta_{\text{inc}}^j = \frac{MSE_j^{\max} - MSE_j^{\text{nom}}}{MSE_j^{\text{nom}}} \cdot 100, \tag{25}$$

$$\delta_{\text{dec}}^j = \frac{MSE_j^{\min} - MSE_j^{\text{nom}}}{MSE_j^{\text{nom}}} \cdot 100, \tag{26}$$

where $MSE_\omega^{\min}, MSE_\omega^{\text{nom}}, MSE_\omega^{\max}$ – the mean square errors calculated for j signal collected during the experiments with decreased ($J_{\min}$), nominal (J_{nom}), and increased ($J_{\max}$) moment of inertia. The above-described formulas were applied to investigate the ripples of the phase current and the angular velocity. The robustness indicator was calculated for phase current ripple as an example of energetic robustness. Based on values listed in Table 5, it can be concluded PI-FCS-MPCC does not significantly increase or decrease current ripples.

Table 5
Robustness indicator $\delta_{\text{dec}}^{i_s}$ and $\delta_{\text{inc}}^{i_s}$ for phase current

DS-FCS-MPC		PI-FCS-MPCC	
$\delta_{\text{dec}}^{i_s}$	$\delta_{\text{inc}}^{i_s}$	$\delta_{\text{dec}}^{i_s}$	$\delta_{\text{inc}}^{i_s}$
–8.72	5.7697	–1.38	0.087

Table 6 presents values for both considered control schemes in three sectors: A – at transient for a step signal, B – at steady-state with T_l, and C – at transient for a ramp signal. Sectors A and B are indicated in Fig. 4 while sector C is indicated in Fig. 5. Indicators $\delta_{\text{inc}}^{\omega}$ and $\delta_{\text{dec}}^{\omega}$ listed in Table 6 refer to increased and decreased moments of inertia. From Fig. 4, it can be seen that DS-FCS-MPC exhibits higher robustness for a lower moment of inertia than PI-FCS-MPCC at transient. Such a behavior is indicated by $\delta_{\text{dec}}^{\omega}$ value. In the case of $\delta_{\text{inc}}^{\omega}$, the values are similar for both schemes. Conversely, for steady-state conditions with T_l, the conclusions are reversed. The last row presents percentage differences in MSE for $J_{\min}$ and $J_{\max}$ compared to J_{nom}. It can be concluded that DS-FCS-MPC is worse than PI-FCS-MPCC when the moment of inertia decreases but greater when it increases. It has been caused by stability and predictable steady-state times for DS-FCS-MPCC. Thanks to that, the difference between δ_{dec} and δ_{inc} is less than in the case of PI-FCS-MPCC.

Table 6
Robustness indicators $\delta_{\text{dec}}^{\omega}$ and $\delta_{\text{inc}}^{\omega}$ for angular velocity

Sector analyzed	DS-FCS-MPC		PI-FCS-MPCC	
	$\delta_{\text{dec}}^{\omega}$ [%]	$\delta_{\text{inc}}^{\omega}$ [%]	$\delta_{\text{dec}}^{\omega}$ [%]	$\delta_{\text{inc}}^{\omega}$ [%]
sector A	39.54	53.05	42.16	52.16
sector B	0.11	0.09	0.01	0.36
sector C	720.37	586.17	242.36	698.96

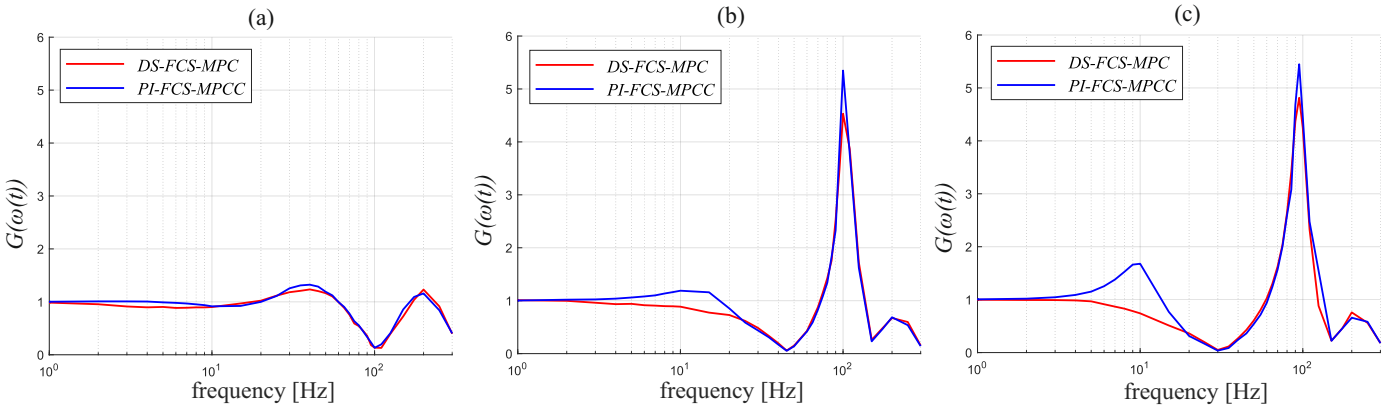

Fig. 6. PMSM drive frequency responses for DS-FCS-MPC and PI-FCS-MPCC excited by sinusoidal reference signal for: (a) $J_{\min}$, (b) J_{nom}, (c) $J_{\max}$

5.4. Frequency responses

In this subsection, Bode's characteristics are presented. These are obtained experimentally for both considered control schemes. Initially, the PMSM was accelerated to 5 rad/s, and after 300 ms, a sinusoidal signal with an amplitude equal to 0.5 rad/s was added to the reference velocity.

In the case of a decreased moment of inertia shown in Fig. 6a, a similar behavior is observed. From Fig. 6b and 6c, differences in the behavior of considered control structures are visible. The proposed DS-FCS-MPC control structure shows better attenuation in the range of 3 to 15 Hz and a lower pick of amplification in resonant frequency equal to 200 Hz. For considered moment of inertia values, characteristics in the range of 1 to 140 Hz are more similar for DS-FCS-MPC, which proves better robustness compared to PI-FCS-MPCC.

6. CONCLUSIONS

In this paper, a direct speed finite control set model predictive control has been proposed for PMSM drive and experimentally validated in both time and frequency domains. The developed control scheme was compared with a cascade control structure based on a finite control set model predictive current control and PI velocity controller. The cost function that provides a high-performance drive operation was successfully developed, and the ABC metaheuristic algorithm has been adopted for the automatic selection of weighting factors.

It was found that PI-FCS-MPCC better compensates load torque, but time response parameters depend on the moment of inertia value. It was particularly evident in the robustness indicator. From the results obtained in the frequency domain, it can be concluded that DS-FCS-MPC is more predictable compared to PI-FCS-MPCC, and therefore, this structure is recommended in applications where robustness and predictable behavior are required. On the other hand, better load torque compensation is observed for PI-FCS-MPCC in the whole frequency domain.

In the future, it is planned to propose predictive control methods with increased robustness and optimized voltage vector selection procedures. Testing the mentioned methods on a robotic arm is also planned.

REFERENCES

[1] T. Tarczewski, R. Szczepanski, K. Erwinski, X. Hu, and L.M. Grzesiak, "A novel sensitivity analysis to moment of inertia and load variations for PMSM drives," *IEEE Trans. Power Electron.*, vol. 37, no. 11, pp. 13 299–13 309, 2022, doi: I10.1109/TPEL.2022.3188404.

[2] M. Rivera, P. Wheeler, J. Rodriguez, E. Zerdali, and S. Toledo Gallardo, "Tutorial: New advances and trends in model predictive control for power electronics and electrical drives," in *Proc. IET Int. Conf. PEMD*, 06 2024.

[3] J. Rodriguez *et al.*, "State of the art of finite control set model predictive control in power electronics," *IEEE Trans. Industr. Inform.*, vol. 9, no. 2, pp. 1003–1016, 2013, doi: 10.1109/TII.2012.2221469.

[4] P. Cortés, M.P. Kazmierkowski, R.M. Kennel, D.E. Quevedo, and J. Rodríguez, "Predictive control in power electronics and drives," *IEEE Trans. Ind. Electron.*, vol. 55, no. 12, pp. 4312–4324, 2008.

[5] H. Yin, C. Ma, H. Wang, Z. Sun, and K. Yang, "Optimal driving torque control strategy for front and rear independently driven electric vehicles based on online real-time model predictive control," *World Electr. Veh. J.*, vol. 15, no. 11, p. 533, 2024, doi: 10.3390/wevj15110533.

[6] S.C. Nwafor, J.N. Eneh, M.I. Ndefo, O.C. Ugbe, H.I. Ugwu, and O. Ani, "An optimal hybrid quadcopter control technique with MPC-based backstepping," *Arch. Control Sci.*, vol. 34, no. 1, pp. 39–62, 2024, doi: 10.24425/acs.2024.149651.

[7] M. Sinner *et al.*, "Experimental testing of a preview-enabled model predictive controller for blade pitch control of wind turbines," *IEEE Trans. Control. Syst. Technol.*, vol. 30, no. 2, pp. 583–597, 2022, doi: 10.1109/TCST.2021.3070342.

[8] J. Peng and M. Yao, "Overview of predictive control technology for permanent magnet synchronous motor systems," *Appl. Sci.*, vol. 13, no. 10, p. 6255, 2023.

[9] X. Jiang *et al.*, "An improved implicit model predictive current control with continuous control set for PMSM drives," *IEEE Trans. Transp. Electr.*, vol. 8, no. 2, pp. 2444–2455, 2022, doi: 10.1109/TTE.2022.3144667.

[10] A.A. Ahmed, B.K. Koh, and Y.I. Lee, "A comparison of finite control set and continuous control set model predictive

control schemes for speed control of induction motors," *IEEE Trans. Ind. Informat.*, vol. 14, no. 4, pp. 1334–1346, 2018, doi: 10.1109/TII.2017.2758393.

[11] Y. Zhang, Z. Zhang, O. Babayomi, and Z. Li, "Weighting factor design techniques for predictive control of power electronics and motor drives," *Symmetry*, vol. 15, no. 6, p. 1219, 2023.

[12] Z. Cui, Z. Zhang, T. Dragicević, and J. Rodríguez, "Dynamic sequential model predictive control of three-level NPC back-to-back power converter PMSG wind turbine systems," in *Proc. IEEE Int. Conf. IECON*, 2020, pp. 3206–3211, doi: 10.1109/IECON43393.2020.9255096.

[13] Q. Dong, B. Wang, L. Xia, Y. Yu, M. Tian, and D. Xu, "Optimized field-weakening operation of PMSM modulated model predictive control using predictive current error margin," *EEE Trans. Energy Convers.*, vol. 39, no. 1, pp. 613–624, 2024, doi: 10.1109/TEC.2023.3305303.

[14] X. Song, H. Wang, X. Ma, X. Yuan, and X. Wu, "Robust model predictive current control for a nine-phase open-end winding PMSM with high computational efficiency," *IEEE Trans. Power Electron.*, vol. 38, no. 11, pp. 13 933–13 943, 2023, doi: 10.1109/TPEL.2023.3309308.

[15] A. Formentini, A. Trentin, M. Marchesoni, P. Zanchetta, and P. Wheeler, "Speed finite control set model predictive control of a PMSM fed by matrix converter," *IEEE Trans. Ind. Electron.*, vol. 62, no. 11, pp. 6786–6796, 2015, doi: 10.1109/TIE.2015.2442526.

[16] C. Zheng, M. Xie, X. Dong, Z. Gong, T. Dragičević, and J. Rodriguez, "Modulated model predictive current control with active damping for LC-filtered PMSM drives," *IEEE J. Emerg. Sel. Topics Power Electron.*, vol. 12, no. 4, pp. 3848–3861, 2024, doi: 10.1109/JESTPE.2024.3408070.

[17] A. Nasr, C. Gu, G. Buticchi, S. Bozhko, and C. Gerada, "A low-complexity modulated model predictive torque and flux control strategy for PMSM drives without weighting factor," *IEEE J. Emerg. Sel. Topics Power Electron.*, vol. 11, no. 2, pp. 1305–1316, 2023, doi: 10.1109/JESTPE.2022.3152652.

[18] R. Fu, "A simple and robust model predictive current control of PMSM using stator current predictor and target-oriented cost function," *IEEE Access*, vol. 10, pp. 100 024–100 032, 2022, doi: 10.1109/ACCESS.2022.3207546.

[19] H. Pan, T. Gu, X. Wang, and K. Xiao, "A new model predictive current control strategy for PMSM based on extended control set and dynamic cost function," *Electr. Eng.*, vol. 107, pp. 3947–3959, 2025, doi: .

[20] M. Zhao, S. Zhang, C. Zhang, X. Li, and Y. Dong, "A parameter robust finite control set model predictive current control based on incremental prediction model for SPMSM drives," *IEEE J. Emerg. Sel. Topics Ind. Electron.*, vol. 5, no. 3, pp. 1292–1302, 2024, doi: 10.1109/JESTIE.2024.3356976.

[21] H.A.G. Al-Kaf, L.M. Halabi, and K.-B. Lee, "A generalized integrated MPC-fuzzy-neural network approach for multilevel inverter fed PMSMs," *IEEE Trans. Ind. Informat.*, vol. 20, no. 2, pp. 2751–2761, 2024, doi: 10.1109/TII.2023.3297662.

[22] O. Asvadi-Kermani, B. Felegari, and H. Momeni, "Adaptive constrained generalized predictive controller for the PMSM speed servo system to reduce the effect of different load torques," *e-Prime Adv. Elect. Eng. Electron. Energy*, vol. 2, p. 100032, 2022.

[23] M. Annoukoubi, A. Essadki, and Y. Akarne, "Model predictive control of multilevel inverter used in a wind energy conversion system application," *e-Prime Adv. Elect. Eng. Electron. Energy*, vol. 9, p. 100717, 2024, doi: 10.1016/j.prime.2024.100717.

[24] M.M. Ismail, M. Al-Dhaifallah, H. Rezk, H.U. Rahman Habib, and S.A. Hamad, "Optimizing battery discharge management of PMSM vehicles using adaptive nonlinear predictive control and a generalized integrator," *Ain Shams Eng. J.*, vol. 15, no. 12, p. 103169, 2024, doi: 10.1016/j.asej.2024.103169.

[25] F. Wang *et al.*, "Design of model predictive control weighting factors for PMSM using gaussian distribution-based particle swarm optimization," *IEEE Trans. Ind. Electron.*, vol. 69, no. 11, pp. 10 935–10 946, 2022, doi: 10.1109/TIE.2021. 3120441.

[26] C. Yao, Z. Sun, S. Xu, H. Zhang, G. Ren, and G. Ma, "ANN optimization of weighting factors using genetic algorithm for model predictive control of PMSM drives," *IEEE Trans. Ind. Appl.*, vol. 58, no. 6, pp. 7346–7362, 2022, doi: 10.1109/TIA.2022.3190812.

[27] T. Tarczewski and L.M. Grzesiak, "An application of novel nature-inspired optimization algorithms to auto-tuning state feedback speed controller for PMSM," *IEEE Trans. Ind. Appl.*, vol. 54, no. 3, pp. 2913–2925, 2018, doi: 10.1109/TIA.2018.2805300.

[28] T. Tarczewski, D. Stojic, R. Szczepanski, L. Niewiara, L.M. Grzesiak, and X. Hu, "Online auto-tuning of multiresonant current controller with nature-inspired optimization algorithms and disturbance in the loop approach," *Appl. Soft Comput.*, vol. 144, p. 110512, 2023.

[29] C. Li, Q. Meng, and T. Shi, "A review on model predictive control strategies for ac motor drives," *IET Electric Power Applications*, vol. 18, no. 1, pp. 1–15, 2024.

[30] P. Wang, F. Niu, L. Guo, S. Huang, and Z. Chu, "Improved robust model predictive control for pmsm using backstepping control and incorporating integral action with experimental validation," *Results in Engineering*, vol. 23, p. 102416, 2024.

[31] Z. Sun, C. Tan, B. Li, A. Song, P. Yu, and M. Hao, "Dual model predictive control strategy of direct-drive pmsm based on sliding mode disturbance observer," *IEEJ Trans. Electr. Electron. Eng.*, vol. 19, no. 4, pp. 527–534, 2024.

[32] H. Lisinski, R. Surus, and T. Tarczewski, "Speed and torque model predictive control for permanent magnet synchronous motor," in *Proc. IEEE Int. Conf. PEMC*, 2024, pp. 1–7, doi: 10.1109/PEMC61721.2024.10726348.

[33] M.H.K. Roni, M. Rana, H. Pota, M.M. Hasan, and M.S. Hussain, "Recent trends in bio-inspired meta-heuristic optimization techniques in control applications for electrical systems: A review," *Int. J. Dyn. Control*, vol. 10, p. 999–1011, 2022, doi: 10.1007/s40435-021-00892-3.